

# High precision measurement of the $^{87}\text{Rb}$ D-line tune-out wavelength

R. H. Leonard,<sup>1</sup> A. J. Fallon,<sup>1</sup> C. A. Sackett,<sup>1</sup> and M. S. Safronova<sup>2,3</sup>

<sup>1</sup>*Physics Department, University of Virginia, Charlottesville, Virginia 22904, USA*

<sup>2</sup>*Department of Physics and Astronomy, University of Delaware, Newark, Delaware 19716, USA*

<sup>3</sup>*Joint Quantum Institute, National Institute of Standards and Technology  
and the University of Maryland, College Park, Maryland, 19716 USA*

(Dated: August 24, 2018)

We report an experimental measurement of a light wavelength at which the ac electric polarizability equals zero for  $^{87}\text{Rb}$  atoms in the  $F = 2$  ground hyperfine state. The experiment uses a condensate interferometer both to find this ‘tune-out’ wavelength and to accurately determine the light polarization for it. The wavelength lies between the D1 and D2 spectral lines at 790.032388(32) nm. The measurement is sensitive to the tensor contribution to the polarizability, which has been removed so that the reported value is the zero of the scalar polarizability. The precision is fifty times better than previous tune-out wavelength measurements. Our result can be used to determine the ratio of matrix elements  $|\langle 5P_{3/2} || d || 5S_{1/2} \rangle / \langle 5P_{1/2} || d || 5S_{1/2} \rangle|^2 = 1.99221(3)$ , a 100-fold improvement over previous experimental values. New theoretical calculations for the tune-out wavelength and matrix element ratio are presented. The results are consistent with the experiment, with uncertainty estimates for the theory about an order of magnitude larger than the experimental precision.

PACS numbers: 03.75.Dg, 37.25.+k, 42.50.Wk

## I. INTRODUCTION

The energy shift experienced by an atom in an off-resonant optical field has found numerous applications in atom trapping, manipulation, and measurement. The light shift can be characterized by a frequency-dependent polarizability, which itself depends in detail on the wave function of the electrons in the atom. Accurate measurements of the polarizability can therefore be used to test atomic theory calculations, or as phenomenological inputs to improve those calculations. Polarizability measurements have a long history of improving our knowledge of atoms in this way [1, 2].

Precise measurements of the polarizability at optical frequencies are technically difficult, because the light shift depends also on the optical intensity and it is hard to accurately determine the intensity *in situ*. However, it is possible to instead measure a light wavelength at which the polarizability equals zero [3–5]. Since these tune-out wavelengths are independent of the intensity, they can be accurately measured by various methods [5–9].

Tune-out wavelengths can be useful for applications involving species-specific optical manipulation [3, 4, 6, 10] and optical Feshbach resonances [9]. In addition, it was recently shown that tune-out wavelengths can be used with an atom interferometer for sensitive detection of rotations and accelerations [11]. Improved knowledge of tune-out wavelengths can lead to better performance in all these applications.

In this paper we report measurement of the tune-out wavelength for  $^{87}\text{Rb}$  near 790 nm, with an accuracy of about 30 fm. This can be compared to the 1.5 to 2 pm precision of previously reported values for this [6] or other tune-out wavelengths [5, 7, 8]. Our result determines the ratio of the D-line dipole matrix elements to an accuracy of 15 ppm, about a factor of 100 bet-

ter than previously known [12–14]. At our precision the measurement is sensitive to many new effects including hyperfine interactions [15], QED effects [16], the Breit interaction [17], and the details of the atomic core and core-valence interactions [4]. The theoretical tools required to handle these challenges are closely related to those needed for interpreting results such as atomic parity violation and electric dipole measurements in terms of fundamental particle properties [18]. Related calculations are also useful for constraining black-body radiation shifts in atomic clocks [19]. Our measurement can thus serve as a useful test for theories, or could be taken as a phenomenological input value for improved results.

## II. EXPERIMENTAL METHOD

For an alkali atom in state  $i$ , the polarizability can be expressed as

$$\alpha_i(\omega) = \frac{1}{\hbar} \sum_f \frac{2\omega_{if}}{\omega_{if}^2 - \omega^2} |d_{if}|^2 + \alpha_c + \alpha_{cv} \quad (1)$$

where the sum is over all excited states  $f$  of the valence electron. The transition frequency between  $i$  and  $f$  is  $\omega_{if}$  and  $d_{if} = \langle f | \mathbf{d} \cdot \hat{\epsilon} | i \rangle$  is the dipole matrix element between  $i$  and  $f$  for light with polarization vector  $\hat{\epsilon}$ . The  $\alpha_c$  term is the polarizability contribution from the core electrons while  $\alpha_{cv}$  expresses the effect of core-valence interactions [4]. At most frequencies,  $\alpha_c$  and  $\alpha_{cv}$  are small compared to the valence contribution. However, tune-out wavelengths occur between pairs of states where the valence contributions largely cancel. Figure 1(a) shows the tune-out wavelength between the D1 and D2 lines of Rb.

Our measurement uses a Bose condensate atom interferometer, similar to that previously described in [20].

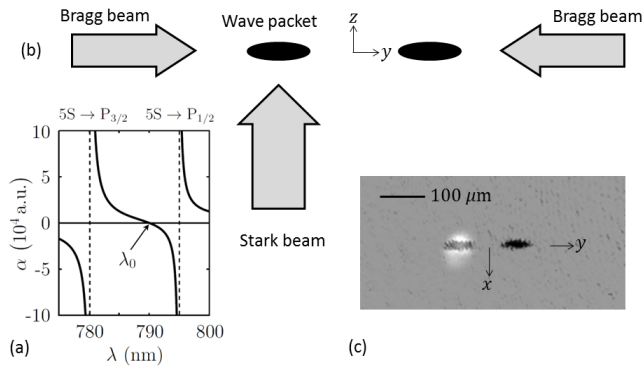


FIG. 1: Schematic of measurement. (a) Theoretical plot of the polarizability  $\alpha$  for  $^{87}\text{Rb}$  near the D1 and D2 transitions. The polarizability crosses zero at the tune-out wavelength  $\lambda_0$ . (b) Optical schematic for the experiment. The two Bragg laser beams form a standing wave that is used to split and recombine a Bose condensate to form an atom interferometer. The Stark laser beam illuminates one of the wave packets in the interferometer to produce a phase shift. (c) Composite image of the atomic wave packets (dark) and the Stark beam (white). Here the wave packet centers are  $130\ \mu\text{m}$  apart after 5 ms of propagation. In (b) and (c), the coordinate axes  $x$ ,  $y$  and  $z$  are illustrated.

A condensate of about  $10^4$   $^{87}\text{Rb}$  atoms is produced and loaded into a weak magnetic trap with harmonic oscillation frequencies of 5.1, 1.1, and 3.2 Hz along the  $x$ ,  $y$ , and  $z$  directions, respectively. The trap uses a time-orbiting potential, with a bias field of 20.0 G rotating in the  $xz$  plane at 12 kHz frequency. Oscillating magnetic gradients provide support against gravity as well as trap confinement.

The atom interferometer is implemented using an off-resonant standing-wave laser propagating along the  $y$  axis, having wave number  $k$ . Via Bragg scattering, a short pulse from this beam can split the atoms into two wave packets traveling with momentum  $\pm 2\hbar k$  [21]. After 10 ms, the wave packets are reflected using another pulse of the Bragg laser, now adjusted to drive the  $|+2\hbar k\rangle \leftrightarrow |-2\hbar k\rangle$  transition. After 20 ms a second reflection pulse is applied, and after another 10 ms, a recombination pulse is applied. By using this symmetric trajectory, both packets traverse identical paths in the trap, which reduces phase shifts and fidelity loss from the trapping potential [20].

The recombination pulse brings a fraction  $N_0/N$  of the atoms back to rest in the center of the trap. We obtain  $N_0/N = [1 + V \cos(\phi + \phi_r)]/2$ , where  $\phi$  is the phase difference developed by the atoms during their separation,  $\phi_r$  is the phase shift of the recombination pulse relative to the initial splitting pulse, and  $V \approx 0.7$  is the visibility. We here set  $\phi_r = \pi/2$  to maximize the sensitivity to  $\phi$ . We measure  $N_0/N$  by allowing the three output wave packets to separate for 40 ms and then observing them via absorption imaging.

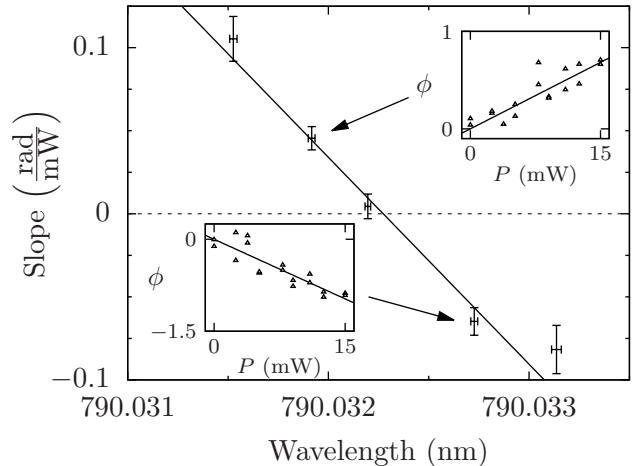


FIG. 2: Sample data. The two inset graphs show interferometric measurements of the phase shift  $\phi$  induced by the Stark beam with power  $P$ . The triangles show individual measurements, which are fit to a line to determine the slope. The large graph shows how the slope varies as a function of the Stark laser wavelength, with the inset graphs corresponding to the indicated points. The vertical error bars are the linear regression errors from the slope fits. The horizontal error bars are the standard deviation of several wavelength measurements made over the course of the slope measurement. The line in the large graph is another linear fit, and the intercept is taken as our measurement result for the tune-out wavelength  $\lambda_0$ . Here  $\lambda_0 = 790.03232\ \text{nm}$ , with a regression error of 50 fm.

To obtain the polarizability  $\alpha$ , we focus another laser beam, traveling along  $z$ , onto one arm of the interferometer. This Stark beam is applied for 20 ms at the start of the interferometer, so that one packet passes through it twice. Figure 1(b) shows the orientation of the beams involved, and Fig. 1(c) is a composite image of the atoms and Stark beam together.

The energy shift  $U$  due to the Stark beam is

$$U = -\frac{1}{2}\alpha \langle \mathcal{E}^2 \rangle = -\frac{\alpha I}{\epsilon_0 c} \quad (2)$$

where  $\mathcal{E}$  is the electric field of the beam,  $I$  is the intensity, and  $c$  is the speed of light. The brackets denote time averaging of the optical field. The light shift induces a phase  $\phi = -(1/\hbar) \int U dt$  proportional to the integrated intensity experienced by the atoms. We use an approximately Gaussian beam with waist  $w \approx 30\ \mu\text{m}$ . For a Stark beam power of  $P$ , this yields  $\phi/(\alpha P) \approx 66\ \text{rad/W}$  for  $\alpha$  in atomic units.

The Stark power can be varied from zero to 15 mW using an acousto-optic modulator. The basic experimental procedure is to set the Stark laser to a given wavelength  $\lambda$  and run the interferometer for different beam powers. The resulting phase is fit to a line to determine the slope, as shown in the Fig. 2 insets. By performing the experiment at different wavelengths, we plot the slope as a

function of  $\lambda$ . A second linear fit yields the wavelength  $\lambda_0$  at which the slope and thus  $\alpha$  equals zero.

### III. LIGHT POLARIZATION EFFECTS

A major complication is that  $\alpha$  depends strongly on the optical polarization of the Stark beam and the orientation of the atomic spin. In general the energy shift can be expressed as [15]

$$U = -\frac{\langle E^2 \rangle}{2} \left\{ \alpha^{(0)} - \mathcal{V} \cos \chi \frac{m_F}{2F} \alpha^{(1)} + \left[ \frac{3 \cos^2 \xi - 1}{2} \right] \frac{3m_F^2 - F(F+1)}{F(2F-1)} \alpha^{(2)} \right\} \quad (3)$$

where the  $\alpha^{(i)}$  are irreducible components of the polarizability, namely the scalar ( $i = 0$ ), vector ( $i = 1$ ) and tensor ( $i = 2$ ) parts. The atom is assumed to be in a particular hyperfine state  $|F, m_F\rangle$  relative to the trap magnetic field direction  $\hat{b} = \mathbf{B}/B$ . Here we have  $F = m_F = 2$ . The angle between the Stark beam wave vector and the magnetic field is  $\chi$ , so  $\cos \chi = \hat{k} \cdot \hat{b}$ . Similarly,  $\cos \xi = \hat{\epsilon} \cdot \hat{b}$  is the projection of the light polarization vector  $\hat{\epsilon}$  onto the magnetic field. Finally  $\mathcal{V}$  is the fourth Stokes parameter for the light, characterizing the degree of circular polarization and expressible as  $\mathcal{V} \cos \chi = i(\hat{\epsilon}^* \times \hat{\epsilon}) \cdot \hat{b}$ .

We are primarily interested in the scalar polarizability  $\alpha^{(0)}$ . The tensor contribution is small but measurable, and will be discussed below. However, the vector contribution can be quite large. For instance, for  $\sigma_+$  polarized light ( $\mathcal{V} = -1$  and  $\chi = 0$ ) the vector term completely eliminates the tune-out wavelength between the D1 and D2 transitions, since the light does not couple our ground state to any states in the D1 manifold. To measure the tune-out wavelength of the scalar term with the desired accuracy, it is necessary to keep  $|\mathcal{V} \cos \chi| < 10^{-5}$ . This is challenging since it is comparable to the performance of the best linear polarizers, and much below the level of polarization that can typically be maintained when a laser beam passes through a vacuum chamber window.

We use two methods to control the vector shift. First, the rotating bias field of the TOP trap causes  $\cos \chi$  in Eq. (3) to alternate sign, with a time average close to zero. We verified that the measurement results did not depend on the phase of the TOP field at the start of the interferometer.

Second, we linearized the light polarization using the interferometer itself. Prior to taking a data set such as in Fig. 2, we ran the experiment with the Stark beam pulsed on and off synchronously with the TOP field. In this way the  $\cos \chi$  term could be made close to +1 or -1. We adjusted the light polarization so that the measured phase shifts for those two cases were equal. The polarization was established with a calcite polarizer, a zero-order half wave plate, and a zero-order quarter wave plate. The wave plates could be set to an accuracy of about  $0.1^\circ$ , corresponding to  $\mathcal{V} \approx 2 \times 10^{-3}$ .

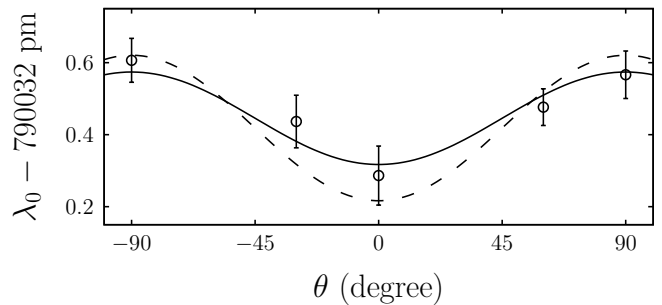


FIG. 3: Effect of tensor polarizability. Data points show tune-out wavelengths  $\lambda_0$ , as a function of the angle  $\theta$  between the linear polarization of the Stark beam and the  $x$  axis of the trap. Each point is an average of several measurements performed as in Fig. 2. For each measurement  $i$  the linear fit error is combined with the estimated polarization error described in the text. The error bars shown are then calculated as  $\sigma^2 = 1/\sum_i \sigma_i^{-2}$ . The solid curve is a sinusoidal fit with a variable offset and amplitude. The dashed curve is a fit with the amplitude constrained to the expected value.

After taking the data set, the polarization check was repeated and any difference between the  $\cos \chi = \pm 1$  phases was used to estimate the polarization drift that occurred during the run. This was converted to a wavelength error using an empirical calibration, and the polarization error was added in quadrature to the regression error calculated as in Fig. 2.

The tensor term in (3) gives rise to a dependence on the angle of the linear light polarization with respect to the trap field, which can be seen in Fig. 3. The polarization was adjusted using the half-wave plate in the Stark beam. For our geometry, the polarization angle  $\theta$  is related to  $\xi$  in (3) via  $\langle \cos^2 \xi \rangle = 0.5 \cos^2 \theta$ , where the brackets denote a time average for the magnetic field.

Near the tune-out wavelength,  $\alpha$  and  $\alpha^{(0)}$  can be accurately approximated as linear functions  $(d\alpha/d\lambda)(\lambda - \lambda_0)$  and  $(d\alpha^{(0)}/d\lambda)(\lambda - \lambda^{(0)})$  respectively. Here  $\lambda_0$  is the measured value shown in Fig. 3 and  $\lambda^{(0)}$  is the desired zero of the scalar term. The tensor contribution to  $d\alpha/d\lambda$  is negligible, so the two derivatives are nearly equal. If we use this and set (3) to zero, we obtain

$$\lambda_0(\theta) = \lambda^{(0)} - \frac{\alpha^{(2)}}{d\alpha^{(0)}/d\lambda} \left( \frac{3}{4} \cos^2 \theta - \frac{1}{2} \right) \quad (4)$$

in the case of  $\mathcal{V} \langle \cos \chi \rangle = 0$ . Fitting to this form, we obtain  $\lambda^{(0)} = 790.032439(35)$  nm and  $\alpha^{(2)}/(d\alpha^{(0)}/d\lambda) = 390(120)$  fm. This fit is shown as the solid curve in Fig. 3.

Alternatively,  $\alpha^{(2)}$  and  $d\alpha^{(0)}/d\lambda$  are almost entirely due to contributions from the 5P manifold, and can be calculated relatively precisely. The derivative term can

be determined from [15]

$$\alpha_{5P}^{(0)} = \frac{10}{\hbar\sqrt{15}} \sum_{J',F'} \frac{|d_{J'}|^2 \omega'}{\omega'^2 - \omega^2} (-1)^{1+F'} (2F' + 1) \times \begin{Bmatrix} 2 & 1 & F' \\ 1 & 2 & 0 \end{Bmatrix} \begin{Bmatrix} F' & 3/2 & J' \\ 1/2 & 1 & 2 \end{Bmatrix}^2 \quad (5)$$

for the  $F = 2$  ground state. Here the sum is over the angular momentum quantum numbers of the 5P states,  $\omega'$  is the transition frequency to the  $|J', F'\rangle$  state, and  $d_{J'} = \langle 5P_{J'} || d || 5S_{1/2} \rangle$  is the reduced dipole matrix element. The  $d_{J'}$  are known to about 500 ppm precision from lifetime and photoassociation measurements [12–14].

Similarly, the tensor term is given by [15]

$$\alpha_{5P}^{(2)} = \frac{20}{\hbar\sqrt{21}} \sum_{J',F'} \frac{|d_{J'}|^2 \omega'}{\omega'^2 - \omega^2} (-1)^{F'} (2F' + 1) \times \begin{Bmatrix} 2 & 1 & F' \\ 1 & 2 & 2 \end{Bmatrix} \begin{Bmatrix} F' & 3/2 & J' \\ 1/2 & 1 & 2 \end{Bmatrix}^2. \quad (6)$$

Evaluating the ratio gives  $\alpha^{(2)}/(d\alpha/d\lambda) = 538.5(4)$  fm, which is larger than the value determined from our fit by about  $1.3\sigma$ . If we constrain the fit to use the calculated value for  $\alpha^{(2)}/(d\alpha/d\lambda)$ , we obtain  $\lambda^{(0)} = 790.032388(29)$  nm, about  $1\sigma$  different from the unconstrained result. The constrained fit gives a  $\chi^2/\text{d.o.f.}$  of 1.2, compared to 0.5 for the unconstrained fit, both of which are reasonable. Since the calculated value for  $\alpha^{(2)}/(d\alpha/d\lambda)$  is expected to be accurate, we report the value obtained from the constrained fit.

#### IV. ERROR ESTIMATION

As noted, each run of the experiment yields a statistical error derived from the linear fits of  $\phi$  vs. intensity, and a polarization error based on the measured polarization drift between the start and end of the run. Each run takes several hours, so we are not confident that the polarization change is linear, or even monotonic, throughout the run. We therefore use the full value of the polarization drift as an error estimate. The polarization drift is in fact the largest error source in the measurement. The average polarization drift error is 126 fm, compared to the average statistical error of 60 fm. Averaging over the 21 measurements used would reduce these values by  $\sqrt{20}$ . However, both errors vary considerably from run to run, so for the analysis we combine the two errors for each data point in Fig. 3. The resulting fits have the uncertainties cited above.

Another error contribution is the calibration uncertainty in our wavelength measurement. We used a Bristol Instruments model 621A wave meter that displayed digits to 1 fm, with results repeatable to about 10 fm. We tested the meter by measuring four known saturated absorption lines in K, Rb, and Cs. The results indicated

a calibration correction of  $-40(5)$  fm at a wavelength of 790 nm. This correction was applied to the data reported here. The full wavelength calibration was performed both at the start and end of data collection, and the two Rb lines were checked periodically throughout the experiment. No significant differences were observed.

A significant source of error is asymmetry in the Stark laser spectrum [5, 8]. The laser diode source produces broadband ASE light [22]. This could be observed through its effect on the spontaneous emission rate of the atoms, and indicated a background spectral density near an atomic resonance of  $S \approx P \times 10^{-17} \text{ Hz}^{-1}$ , in terms of the total Stark power  $P$ . This is large enough to shift  $\lambda_0$ , depending on the spectral distribution. We controlled the effect by spectrally filtering the beam using a diffraction grating and pinhole. Using a 0.4 nm  $\approx$  200 GHz filter bandwidth, and assuming a 10% variation of the spectrum across that bandwidth, the estimated spectral density would produce a shift of about 0.1 fm. However, it is possible that the spectral density near 790 nm is larger than that at the atomic resonance. Such low spectral power levels are difficult to measure directly, so we quantified the effect by comparing our  $\lambda_0$  results obtained with 0.2 nm and 0.4 nm filter bandwidths. About half our data was taken in each configuration. No measurable difference was observed, within our 30 fm precision. The expected error would scale as the bandwidth squared, indicating that the error for the smaller bandwidth configuration was less than 10 fm. We use this as the uncertainty from the effect, though we expect it is an overestimate. Asymmetry in the tails of the laser line itself could similarly shift the measurement, but this could be ruled out at the 1-fm level using an optical spectrum analyzer.

Uncertainty in the trap magnetic field can affect our result by changing the value of  $\langle \cos^2 \xi \rangle$  in the tensor term. The most significant effect is if the magnitude of the bias field varies as it rotates. We were able to place a limit of 2% on such variations by measuring the Zeeman linewidth of the trapped atoms using rf spectroscopy. In the worst case, this would induce a 5 fm shift on the value of  $\lambda^{(0)}$ . Other effects are smaller, including distortions from a dc background field of less than 1 G, and angular misalignment of less than 3 degrees between the Stark beam polarization measurement and the plane of the bias field.

The hyperpolarizability of the atoms characterizes the nonlinear Stark effect. We estimate the effect by treating the  $P_{1/2}$  and  $P_{3/2}$  transitions as two-level systems in the rotating wave approximation, and summing the resulting energy shifts. At the tune-out wavelength, we obtain a net shift

$$\delta U \approx -\frac{|d_{1/2}|^4 \mathcal{E}^4}{32\hbar^3 \Delta^3} \quad (7)$$

where  $\Delta$  is the detuning from the  $P_{1/2}$  transition and  $\mathcal{E}$  is the Stark field amplitude. At the maximum intensity used, this changes  $\lambda^{(0)}$  by only about 1 fm.

TABLE I: Estimated error contributions to  $\lambda^{(0)}$ . The entries for statistical error and polarization drift report the average errors for each type, divided by the square root of the number of measurements. In the analysis, both errors were combined at each data point to give the reported combined error in the result.

Source	Error (fm)
Statistical	13
Polarization drift	28
Stat and polz. combined	29
Broadband spectrum	10
Wavemeter calibration	5
Trap field variation	5
dc background field	2
Hyperpolarizability	1
Total	32

The effect of interatomic interactions is negligible, as the chemical potential of the condensate is only about  $2\pi\hbar \times 10$  Hz. The Zeeman shift from the trap field, however, is not small. By summing the contributions of the individual Zeeman transitions, we calculate that it shifts the measured tune-out wavelength blue by 36 fm, so we have added this amount to our reported values to give the estimated zero-field result. From rf spectroscopy we know the bias field magnitude of 20.0(2) G very accurately, so we estimate the error in this shift to be less than 1 fm.

Our error analysis results are summarized in Table I. We sum the errors in quadrature to give our final reported one-sigma uncertainty of 32 fm.

## V. COMPARISON TO THEORY

One other experimental measurement of this tune-out wavelength exists, by Lamporesi *et al.* who obtained 790.018(2) nm [6]. Our result is in considerable ( $7\sigma$ ) disagreement, but those authors did not report any special effort to control the light polarization. We expect therefore that their result is for the particular combination of scalar and vector polarizabilities that was relevant to their experiment.

We can however make a useful comparison to theory. We first describe how the theoretical result was obtained. In the decomposition of Eq. 1, the core terms  $\alpha_c$  and  $\alpha_{vc}$  are approximately static and are calculated in the random-phase approximation [23]. The valence term for the  $5S$  state can be expressed in atomic units as

$$\alpha_v(\omega) = \frac{1}{3} \sum_k \frac{\langle k || d || 5S \rangle^2 (E_k - E_{5S})}{(E_k - E_{5S})^2 - \omega^2}, \quad (8)$$

where  $k = nP_{1/2}$  and  $nP_{3/2}$ . Up to  $n = 12$  we evaluate discrete terms in this sum using experimental values for the state energies  $E$ . Experimental matrix elements from Ref. [12] are used for the  $5S - 6P$  transitions

TABLE II: Breakdown of the contributions to the  $5S$  polarizability in Rb at  $\lambda = 790.02568$  nm. Reduced matrix elements  $d$  and polarizability contributions are given in atomic units. Experimental matrix elements from Ref. [7] are used for the  $5S - 6P$  transitions; remaining matrix elements are from the all-order calculations [7, 23]. Uncertainties are given in parenthesis. Experimental energies  $\Delta E$  are measured from the ground state and given in  $\text{cm}^{-1}$  [25].

Contr.	$\Delta E$	$d$	$\alpha_0$
$5P_{1/2}$	12578.951	4.2199	-8233.6
$6P_{1/2}$	23715.081	0.3235(9)	0.451(3)
$7P_{1/2}$	27835.05	0.115(3)	0.044(2)
$8P_{1/2}$	29834.96	0.060(2)	0.011(1)
$9P_{1/2}$	30958.91	0.037(3)	0.004(1)
$10P_{1/2}$	31653.85	0.026(2)	0.002
$11P_{1/2}$	32113.55	0.020(1)	0.001
$12P_{1/2}$	32433.50	0.016(1)	0.001
$(n > 12)P_{1/2}$			0.022(22)
$5P_{3/2}$	12816.54939	5.9550	8222.9
$6P_{3/2}$	23792.591	0.5230(8)	1.173(4)
$7P_{3/2}$	27870.14	0.202(4)	0.135(6)
$8P_{3/2}$	29853.82	0.111(3)	0.037(2)
$9P_{3/2}$	30970.19	0.073(5)	0.015(2)
$10P_{3/2}$	31661.16	0.053(4)	0.008(1)
$11P_{3/2}$	32118.52	0.040(3)	0.004(1)
$12P_{3/2}$	32437.04	0.033(2)	0.003
$(n > 12)P_{3/2}$			0.075(75)
Core + vc			8.709(93)
Total			0.001

while all other matrix elements use the all-order calculations of [23]. The details of the methods are discussed in [24]. While experimental values are available for the  $5S - 5P$  matrix elements [12], the theoretical values are estimated to have a more accurate ratio, which is most important here. For  $n > 12$ , the remaining ‘tail’ contributions are calculated in the Dirac-Hartree-Fock approximation. The state energies and matrix elements are listed in Table II. Using these values, the tune-out wavelength is predicted to lie at  $\lambda^{(0)} = 790.02568$  nm as indicated.

The uncertainty in the theoretical value is dominated by uncertainty in the  $5P$  matrix elements. In Table III we compare the matrix elements obtained using various approximations [23]. All of the methods are intrinsically relativistic. The calculations in Table III of the tune-out wavelength differ only in the values of these two matrix elements, with all other values taken from Table II.

The most accurate methods are expected to be the four all-order calculations SD, SDpT,  $SD_{sc}$ , and  $SDpT_{sc}$ . We take the average of these as the final theoretical values, and use them to calculate  $\lambda^{(0)} = 790.0261(7)$  nm. The uncertainty is estimated from the spread in the four values. While the scaling ( $SD_{sc}$ , and  $SDpT_{sc}$ ) technique is supposed to account for a class of missing correlation effects, the scaling affects only about half of the correlation correction in this transition. Therefore we use the full spread of the values as our error estimate to allow for

TABLE III: Reduced electric-dipole matrix elements for the  $5S - 5P_J$  transitions [23], values of the tune-out wavelength  $\lambda^{(0)}$ , the matrix element ratio  $R$ . Theoretical methods: DF is the lowest-order Dirac-Hartree-Fock, II and III are second- and third-order many-body perturbation theory values, SD and SDpT are *ab initio* all-order values calculated in the single-double approximation and with inclusion of the partial triple contributions, and  $SD_{sc}$ ,  $SDpT_{sc}$  are corresponding scaled all-order values. Experimental values are averages of several experimental measurements [12–14].

	DF	II	III	SD	$SD_{sc}$	SDpT	$SDpT_{sc}$	Expt.
$5S - 5P_{1/2}$	4.8189	4.5981	4.1855	4.2199	4.2535	4.2652	4.2498	4.233(2)
$5S - 5P_{3/2}$	6.8017	6.4952	5.9047	5.955	6.0031	6.0196	5.9976	5.978(4)
$\lambda^{(0)}$ (nm)	790.02603	790.03155	790.02380	790.02568	790.02636	790.02632	790.02607	790.031(6)
$R$	1.9922	1.9954	1.9902	1.9914	1.9919	1.9918	1.9917	1.995(3)

TABLE IV: Reduced electric-dipole matrix elements for the  $5S - 5P_J$  transitions and the corresponding line strength ratio  $R$ .

	DF	DF+Breit	DF+QED
$5S - 5P_{1/2}$	4.8189	4.8192	4.82038
$5S - 5P_{3/2}$	6.8017	6.8023	6.80384
$R$	1.9922	1.9923	1.9923

the effects missed by scaling. We note that this uncertainty estimation is approximate since we are attempting to account for unknown correlation effects due to triple, quadrupole, and higher excitations.

The estimated uncertainty in  $\alpha$  from all of the non-5P contributions is about 0.12 au. Via the derivative  $d\lambda/d\alpha = -397$  fm/au, this leads to a wavelength error of 50 fm, about ten times smaller than the uncertainty from the 5P levels. The net value of the non-5P contributions does give a significant shift of -4.2 pm, mainly from the core polarizability.

The wavelength value determined above does not include the effects of hyperfine structure. This can be incorporated using Eq. (5) for the 5P levels, using the theoretical estimate for the dipole matrix elements. The effect of hyperfine structure from all other levels is negligible. This yields  $\lambda^{(0)} = 790.0312(7)$  nm, in reasonable agreement with the experimental value of 790.032388(32) nm. The values differ by  $1.7\sigma$ , with the theoretical uncertainty about twenty times larger than that of the experiment.

As noted, the 5P matrix elements themselves contribute primarily through their ratio

$$R = \frac{|\langle 5P_{3/2} || d || 5S \rangle|^2}{|\langle 5P_{1/2} || d || 5S \rangle|^2}. \quad (9)$$

This is useful, because the theoretical accuracy of the ratio is better than that of the individual matrix elements since a large fraction of the correlation corrections cancel. This can be seen in the calculations in Table III. Using the same error estimation procedure as above, we obtain a ratio  $R = 1.9917(5)$ .

None of the matrix element values in Table III include Breit or QED corrections. We evaluate the importance of these effects in the lowest-order DF approximation and summarize the resulting values in Table IV. First, we

carry out the DF calculation with the Breit interaction included on the same footing with the Coulomb interaction (see, for example, Ref. [17]). The resulting values are listed in the column labeled “DF+Breit.” Then, we carry out the DF calculation with the inclusion of the QED model potential, constructed as described in Ref. [16]. The Breit interaction is excluded in this calculation to separate the two effects. We find that both Breit and QED corrections are five times smaller than our uncertainty in the correlation contribution to the ratio. However, we include the shifts in our estimate  $R = 1.9919(5)$ .

An experimental determination of the matrix element ratio requires some theoretical input [5]. The scalar polarizability can be expressed

$$\alpha^{(0)} = A + |d_{1/2}|^2 (K_{1/2} + K_{3/2}R) \quad (10)$$

where  $A$  includes  $\alpha_c$ ,  $\alpha_{cv}$ , and contributions from valence states above  $5P$ . Using the values from Table II gives  $A = 10.70(12)$  au. The experimental value for  $d_{1/2}$  is 4.233(2) au [12–14]. The coefficients  $K_{J'} \equiv \alpha_{5P_{J'}}^{(0)} / |d_{J'}|^2$  can be obtained from Eq. (5) and our result for  $\lambda^{(0)}$ . Setting  $\alpha^{(0)} = 0$  and solving for  $R$  yields 1.99221(3). This differs from our theory result by  $0.6\sigma$ , and is about twenty times more accurate. Both values are consistent with the ratio of the previous experimental matrix elements,  $R = 1.995(3)$ .

## VI. CONCLUSIONS

Our measurement of the  $^{87}\text{Rb}$  790 nm tune-out wavelength illustrates that tune-out wavelength spectroscopy can provide high precision information about atomic matrix elements. As one immediate application, our measurement of the matrix element ratio provides a moderate improvement to the absolute values of the  $5P_{1/2}$  and  $5P_{3/2}$  matrix elements. Each of these elements has been determined with about 0.1% precision in three previous investigations [12–14]. Our 15 ppm determination of the ratio allows all six measurements to be combined, reducing the total estimated error in each element by about a factor of  $\sqrt{2}$ , as seen in Fig. 4. The resulting best values are  $d_{1/2} = 4.2339(16)$  and  $d_{3/2} = 5.9760(23)$ . Precise

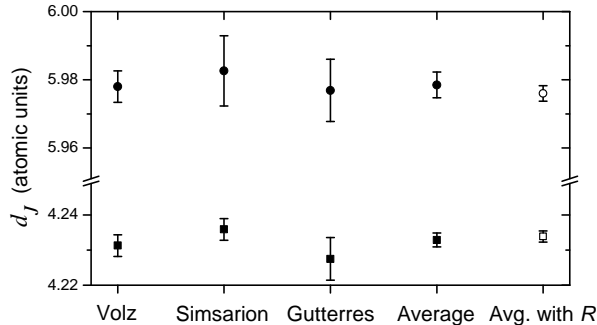


FIG. 4: Matrix element values. The points show various determinations of the  $d_J = \langle 5P_J || d || 5S_{1/2} \rangle$  matrix elements, for  $J = 1/2$  (squares) and  $J = 3/2$  (circles). The first three points are measurements by Volz *et al.* [12], Simsarian *et al.* [13] and Gutterres *et al.* [14]. The fourth point is the error-weighted average from the three groups. The fifth point (hollow) is the error-weighted average of all six measurements, with the constraint  $d_{3/2}^2/d_{1/2}^2 = R = 1.99219$  obtained in the present work.

knowledge of  $R$  may permit yet further improvements using the technique of Ref. [26].

Our results have several important conclusions in regards to the atomic theory calculations. First, the good agreement between the measured and calculated values of  $\lambda^{(0)}$  provides confirmation of the theoretical accuracy. Prior to our measurement, the theory result was about five times more accurate than the best experimental estimate, making the theoretical prediction difficult to check. In particular, our result validates the procedure used to estimate the theoretical error, since the error accurately reflects the disagreement with experiment. This type of error validation is valuable since theoretical error estimates are both challenging and important to obtain.

Second, we demonstrate that the ratio of matrix ele-

ments can be a useful measure of the accuracy of theoretical approaches to include electron correlations. Note that the second-order and third-order values in Table III are outside of the theory uncertainty estimate, and disagree significantly with the experimental result. These methods are thus confirmed to be less accurate than the all-order techniques.

Third, the accuracy of the experimental ratio value is sufficient to test the Breit and QED effects if a more accurate treatment of correlations is carried out. It may be possible to achieve this in the full triple coupled-cluster approach used to treat Cs parity violation [27]. If successful, this would help support the theoretical methods and thus clarify the parity violation results [16, 17].

The method we have demonstrated can readily be applied to other tune-out wavelengths in Rb, which we hope to pursue in future work. We hope in this way that the Rb atom can be established as a well-known reference atom for testing theoretical techniques. The significant advance in experimental precision should provide a useful benchmark for some time to come.

More generally our method can be applied to any Bose-condensed atomic species, which includes many species used in precision measurement applications. We hope that the improved knowledge of matrix elements made possible will prove valuable.

## Acknowledgments

We are grateful to A. Cronin for helpful discussions and comments on the manuscript, and to V. Dzuba for the use of his QED code. The Virginia group was supported by the National Science Foundation Grant No. 1312220, NASA Grant No. 1502012, and the Jefferson Scholars Foundation. This research was performed in part under the sponsorship of the US Department of Commerce, National Institute of Standards and Technology.

- 
- [1] H. Gould and T. M. Miller, in *Advances in Atomic, Molecular, and Optical Physics, Vol. 51*, edited by P. R. Berman, C. C. Lin, and H. Walther (Elsevier, Amsterdam, 2005), p. 343.
  - [2] J. Mitroy, M. S. Safronova, and C. W. Clark, *J. Phys. B: At. Mol. Opt. Phys.* **43**, 202001 (2010).
  - [3] L. J. LeBlanc and J. H. Thywissen, *Phys. Rev. A* **75**, 053612 (2007).
  - [4] B. Arora, M. S. Safronova, and C. W. Clark, *Phys. Rev. A* **84**, 043401 (2011).
  - [5] W. F. Holmgren, R. Trubko, I. Hromada, and A. D. Cronin, *Phys. Rev. Lett.* **109**, 243004 (2012).
  - [6] G. Lamporesi, J. Catani, G. Barontini, Y. Nishida, M. Inguscio, and F. Minardi, *Phys. Rev. Lett.* **104**, 153202 (2010).
  - [7] C. D. Herold, V. D. Vaidya, X. Li, S. L. Rolston, J. V. Porto, and M. S. Safronova, *Phys. Rev. Lett.* **109**, 243003 (2012).
  - [8] B. M. Henson, R. I. Khakimov, R. G. Dall, K. G. H. Baldwin, L.-Y. Tang, and A. G. Truscott, *Phys. Rev. Lett.* **115**, 043004 (2015).
  - [9] L. W. Clark, L.-C. Ha, C.-Y. Xu, and C. Chin (2015), arXiv:1506:01766 [cond-mat.quant.gas].
  - [10] P. Schneeweiss, F. L. Kien, and A. Rauschenbeutel, *New J. Phys.* **16**, 013014 (2014).
  - [11] R. Trubko, J. Greenberg, M. T. S. Germaine, M. D. Gregoire, W. F. Holmgren, I. Hromada, and A. D. Cronin, *Phys. Rev. Lett.* **114**, 140404 (2015).
  - [12] U. Volz and H. Schmoranzler, *Physica Scripta T* **65**, 48 (1996).
  - [13] J. E. Simsarian, L. A. Orozco, G. D. Sprouse, and W. Z. Zhao, *Phys. Rev. A* **57**, 2448 (1998).

- [14] R. F. Gutterres, C. Amiot, A. Fioretti, C. Gabbanini, M. Mazzoni, and O. Dulieu, *Phys. Rev. A* **66**, 024502 (2002).
- [15] F. L. Kien, P. Schneeweiss, and A. Rauschenbeutel, *Eur. Phys. J. D* **67**, 92 (2013).
- [16] V. V. Flambaum and J. S. M. Ginges, *Phys. Rev. A* **72**, 052115 (2005).
- [17] V. A. Dzuba, V. V. Flambaum, and M. S. Safronova, *Phys. Rev. A* **73**, 022112 (2006).
- [18] V. A. Dzuba and V. V. Flambaum, *Int. J. Mod. Phys. E* **21**, 1230010 (2012).
- [19] M. S. Safronova, M. G. Kozlov, and C. W. Clark, *IEEE Trans. Ultrason., Ferroelect., Freq. Control* **59**, 439 (2012).
- [20] J. H. T. Burke, B. Deissler, K. J. Hughes, and C. A. Sackett, *Phys. Rev. A* **78**, 023619 (2008).
- [21] K. J. Hughes, B. Deissler, J. H. T. Burke, and C. A. Sackett, *Phys. Rev. A* **76**, 035601 (2007).
- [22] W. W. Chow and R. R. Craig, *IEEE J. Quant. Elect.* **16**, 1363 (1990).
- [23] M. S. Safronova and U. I. Safronova, *Phys. Rev. A* **83**, 052508 (2011).
- [24] M. S. Safronova and W. R. Johnson, *Adv. At. Mol., Opt. Phys.* **55**, 191 (2007).
- [25] Kramida, A, Ralchenko, Yu, Reader, J, and NIST ASD Team (2012). NIST Atomic Spectra Database (ver. 5.0), [Online]. Available: <http://physics.nist.gov/asd> [2013, June 24]. National Institute of Standards and Technology, Gaithersburg, MD.
- [26] A. Derevianko and S. G. Porsev, *Phys. Rev. A* **65**, 053403 (2002).
- [27] S. G. Porsev, K. Beloy, and A. Derevianko, *Phys. Rev. Lett.* **102**, 181601 (2009).